# Effects of strong laser fields on hadronic helium atoms

Han-Chieh Lee
*Institute of Physics, National Chiao-Tung University, Hsinchu 30010, Taiwan*
*and United Microelectronics Corporation, Hsinchu 30078, Taiwan*

Tsin-Fu Jiang*
*Institute of Physics, National Chiao-Tung University, Hsinchu 30010, Taiwan*
(Received 9 December 2013; revised manuscript received 24 May 2015; published 30 December 2015)

The metastable hadronic helium atoms in microseconds lifetime are available in laboratory, and two-photon spectroscopy was reported recently. This exotic helium atom has an electron in the ground state and a negative hadron rotating around the helium nucleus. We theoretically study the excitation on hadronic helium by femtosecond pulse and elucidate the influence of moleculelike structure and rotation behavior on the photoelectron spectra and high-order harmonic generation. Because of the moleculelike structure, the electronic ground state consists of several angular orbitals. These angular orbitals can enhance photoelectron spectra at high energies, and also influence the harmonic generation spectra considerably. In particular, the harmonic spectra can occur at even harmonic orders because of the transition between these angular orbitals and continuum states. On the other side, the rotation behavior of hadron can induce a frequency shift in the harmonic spectra. The magnitude of the frequency shift depends on the orbiting speed of the hadron, which is considerable because the rotation period is in a few femtoseconds, a time scale that is comparable to that of infrared laser and is feasible in current laser experiments.

DOI: 10.1103/PhysRevA.92.063429 PACS number(s): 32.80.Rm, 36.10.Gv, 33.60.+q, 42.65.Ky

## I. INTRODUCTION

The experiments of the ASACUSA group [1–3] in CERN [4] demonstrated that by impinging antiproton beams on liquid or gaseous helium, most antiprotons are captured and about 3% of them form metastable atoms ($\overline{p}\mathrm{He}^+$) that have a lifetime of a few microseconds. Similar results were observed for the incidence of negative hadron beams, such as kaons ($K^-$) or pions ($\pi^-$), which form metastable hadronic helium atoms ($X^-\mathrm{He}^+$) [5], too. The origin of longevities of the mesonic atoms, known from the bubble-chamber experiment, was explained by Condo [6] and Russell [7] during the 1960s. In the formed hadronic atom, the quantum state can be distributed broadly; however, the captured hadron favors to occupy a quantum state of the large principle quantum number $n_x \sim (M_r/m_e)^{1/2}$ [8] [e.g., $n_x$ of $(\overline{p}\mathrm{He}^+) \sim 38$] because the orbital has a binding energy similar to that of the replaced electron, where $M_r$ is the reduced mass of $X^-\mathrm{He}^+$ and $m_e$ is the mass of the electron. The decay mechanism of hadronic helium was carefully studied [3,8,9]. The circular state ($n_x$,$l_x = n_x - 1$) is more stable than other states and can be modeled semiclassically.

Hadronic heliums were intensively investigated [10]. Namely, the antiproton capture process has been studied experimentally [1,2,11–13] and theoretically [14,15]. A recent two-photon experiment demonstrated the antiproton-to-electron mass ratio with a similar precision to that of proton-to-electron mass ratio [16] and the transition frequency of antiprotonic helium with agreement to that of the highly precise theoretical calculations [17]. These studies provide critical data for examining fundamental physics laws in antimatter such as charge, parity, time reversal symmetry [13], and quantum electrodynamics. Recently, the three-body mass polarization effect that induced a resonance energy difference by using V-shaped coordinates and Jacobi coordinates was resolved by sophisticated calculations [18,19].

Hadronic helium is an unusual three-body system which consists of a helium nucleus, a hadron, and an electron. On one hand, hadronic helium is a kind of exotic *atom*, but the heavy hadron mass and nucleus make it similar to a two-center diatomic *molecule*. On the other hand, the captured hadron is negatively charged unlike a diatomic molecule which has two positive nuclei. Because of the dual atomic and molecular property, hadronic helium was called *atomcule* [3]. Furthermore, the captured hadron is moving around the helium nucleus in the field of an electron cloud. The orbiting speed of hadron is particularly fast. According to the hadron-to-electron angular speed ratio $\sim 1/l_x$, the orbiting period of the hadron is in the order of femtoseconds, while $l_x$ is in the order of several tens. This orbiting time scale approaches the optical cycle of an infrared (IR) laser. Thus, possible coupling effects between the hadronic rotation and the IR laser can occur. As shown in Ref. [16], the hadronic atom is amenable for laser spectroscopy; thus, the interactions of atomcules with current ultrashort laser pulses could be a new subject in quantum dynamics to explore. Intense and ultrashort laser pulse interactions involving atoms and molecules has been a growing field in atomic, molecular, and optical physics. Prominent phenomena such as above-threshold ionization (ATI) and high-order harmonic generations (HHG) have generated much new interest [20–27]. However, to our knowledge, such research on hadronic helium has not yet been performed.

In this paper we theoretically study the strong-field phenomena of hadronic heliums excited by IR laser pulses. Among the plenty of hadron trapping conditions, we consider the most probable circular state, and elucidate the circular-state effect on the ATI and HHG spectra. Because of the molecularlike structure, the electronic ground state is no longer spherical but consists of a number of angular momentum components. The

*tfjiang@nctu.edu.tw

 

presence of these angular orbitals can enhance ATI spectra at high photoelectron energies. The enhancement depends on the hadronic rotation speed. As the rotation speed increases, the enhanced effect is strengthened. As for the HHG, because of the molecularlike structure, the hadronic helium is no longer limited to generate odd harmonics only, but also allows the generation of even-order harmonics, just like the heteronuclear diatomic molecules. Moreover, the HHG in hadronic helium can also emit harmonics that are not an integer of IR frequency because of hadronic rotation dynamics. The rotation effect makes a frequency shift in the HHG spectra. The frequency shift is dependent on the hadronic rotation frequency and considerable because of a fast hadronic rotation period, which is comparable to an IR optical cycle.

This paper is organized as follows. In Sec. II we describe the theoretical method including (i) the metastable state of the hadronic helium atom, (ii) the transformation from the rotating coordinates system to the laboratory system, and (iii) the electronic excitation by the strong laser pulse. In Sec. III we present the ATI and the HHG spectra to elucidate the moleculelike effect and the rotational effect. Finally, conclusions are drawn in Sec. IV. Unless otherwise stated, atomic units (a.u.), i.e., $m_e = e = \hbar = 1$, are used in this paper.

## II. METHODOLOGY

### A. The metastable state of the hadronic helium atom

Figure 1(a) shows the semiclassical picture of circular motion for a hadronic helium. In the laboratory frame $S$, a hadron $X^-$ rotates around the coordinate origin at which the nucleus stands. Instead, if we change to the rotating frame $S'$ as plotted, the hadron $X^-$ becomes fixed at the $z'$ axis. This is helpful to solve this problem because the system can be reduced to a static Hamiltonian description, where we can find the total wave function of the hadronic helium in a proper method. With Fig. 1(b), the Hamiltonian in the rotating frame $S'$ can be written down as

$$H = -\frac{1}{2M_r}\nabla^2_{\mathbf{R}'} - \frac{1}{2}\nabla^2_{\mathbf{r}'} + V(\mathbf{r}',\mathbf{R}') - \frac{2}{R'}, \tag{1}$$

where $V(\mathbf{r}',\mathbf{R}') = -\frac{2}{r'} + \frac{1}{|\mathbf{r}'-\mathbf{R}'|}$, and $M_r$ is the reduced mass of hadron and the helium nucleus. The mass polarization term is neglected here because it provides a small contribution to both the energy structures and the capture cross sections for such a system [19]. Within the Born-Oppenheimer (BO) approximation, the wave function for the Hamiltonian can be written as $\Psi(\mathbf{r}',\mathbf{R}') = \psi(\mathbf{r}';\mathbf{R}')\chi(\mathbf{R}')$, where $\psi(\mathbf{r}';\mathbf{R}')$ and $\chi(\mathbf{R}')$ are the electronic and hadronic wave functions, respectively. They satisfy

$$-\frac{1}{2}\nabla^2_{\mathbf{r}'}\psi + V(\mathbf{r}',\mathbf{R}')\psi = E(R')\psi, \tag{2a}$$

$$-\frac{1}{2M_r}\nabla^2_{\mathbf{R}'}\chi + \left[E(R') - \frac{2}{R'}\right]\chi = \varepsilon\chi. \tag{2b}$$

The validity of the BO approximation depends on the characteristic time of the $He^+$-$X^-$ vibration and the electron motion. The ratio of vibration time scale to electron motion for targets considered here ($\bar{p}He^+$ and $K^-He^+$) at the circular state can be at two orders of magnitude as showed by Shimamura [9], thus justifying the approximation. To solve Eq. (2a), the potential $\frac{1}{|\mathbf{r}'-\mathbf{R}'|}$ is expanded as $\sum_{k=0}^{\infty}\frac{r'^k_<}{r'^{k+1}_>}P_k(\cos\theta')$, where $P_k(\cos\theta')$ is the Legendre polynomial of order $k$, $r'_< = \min(r',R')$ and $r'_> = \max(r',R')$. The electronic wave function

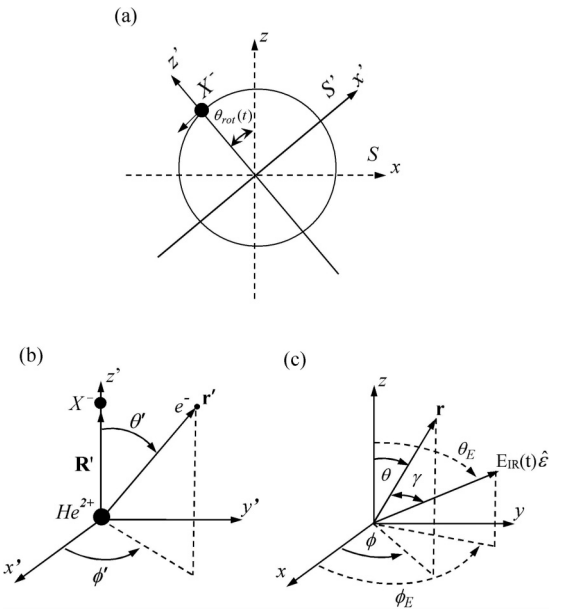


FIG. 1. (a) Schematic diagrams of hadronic helium for the transformation between the laboratory frame $S$ and the rotating frame $S'$. (b) Geometric description of the $X^-He^+$ atom for the interaction among the $He^{2+}$ ion, hadron $X^-$, and electron at the rotating frame $S'$. (c) Geometrical description of the $X^-He^+$ atom in the presence of an electric field.

TABLE I. Comparison between electronic eigenenergies of $\bar{p}He^+$ in the molecular Born-Oppenheimer model by Shimamura [9] and the present results.

| | $1\sigma$ | | $2\sigma$ | |
|---|---|---|---|---|
| $R$ | Shimamura | This work | Shimanura | This work |
| 0.05 | −0.5031900 | −0.5031880 | −0.1253978 | −0.1253976 |
| 0.10 | −0.5123196 | −0.5123131 | −0.1265262 | −0.1265254 |
| 0.15 | −0.5269067 | −0.5268941 | −0.1282993 | −0.1282978 |
| 0.20 | −0.5465679 | −0.5465653 | −0.1306356 | −0.1306353 |
| 0.25 | −0.5709082 | −0.5708841 | −0.1334506 | −0.1334479 |
| 0.30 | −0.5994601 | −0.5994285 | −0.1366563 | −0.1366529 |
| 0.35 | −0.6316630 | −0.6316229 | −0.1401650 | −0.1401609 |
| 0.40 | −0.6668734 | −0.6668161 | −0.1438933 | −0.1438876 |
| 0.45 | −0.7043992 | −0.7043573 | −0.1477675 | −0.1477634 |
| 0.50 | −0.7435419 | −0.7434934 | −0.1517257 | −0.1517212 |
| 0.55 | −0.7836382 | −0.7835822 | −0.1557197 | −0.1557147 |
| 0.60 | −0.8240915 | −0.8240098 | −0.1597134 | −0.1597062 |
| 0.65 | −0.8643914 | −0.8643242 | −0.1636814 | −0.1636756 |
| 0.70 | −0.9041202 | −0.9040266 | −0.1676070 | −0.1675991 |
| 0.75 | −0.9429518 | −0.9428656 | −0.1714796 | −0.1714724 |
| 0.80 | −0.9806429 | −0.9805620 | −0.1752934 | −0.1752867 |
| 0.85 | −1.0170227 | −1.0169392 | −0.1790456 | −0.1790386 |
| 0.90 | −1.0519803 | −1.0518962 | −0.1827354 | −0.1827283 |
| 0.95 | −1.0854533 | −1.0853879 | −0.1863632 | −0.1863576 |
| 1.00 | −1.1174174 | −1.1173550 | −0.1899302 | −0.1899248 |

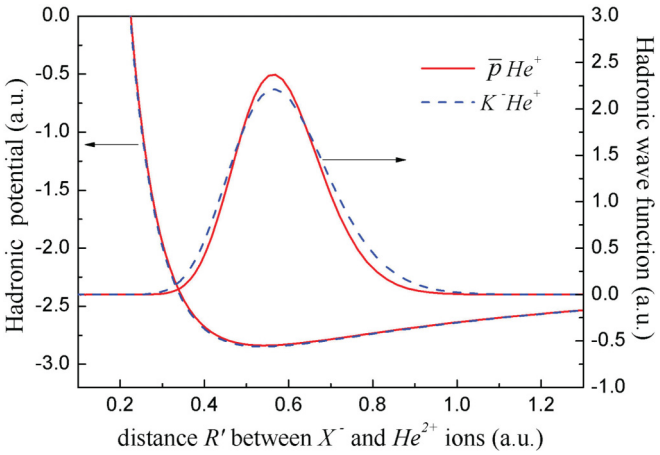


FIG. 2. (Color online) Hadronic potential (left axis) and hadronic wave function (right axis) as a function of distance $R'$ between hadron $X^-$ and the $He^{2+}$ ion for the $\bar{p}He^+$ atom (red-solid line) and the $K^-He^+$ atom (blue-dashed line).

is decomposed by $\psi(\mathbf{r}';\mathbf{R}') = \sum_j \sqrt{\frac{2j+1}{2}} \frac{u_j(r';R')}{r'} P_j(\cos\theta')$. Integrating Eq. (2a) over the angle yields

$$\left[-\frac{1}{2}\frac{\partial^2}{\partial r'^2} + \frac{l(l+1)}{2r'^2} - \frac{2}{r'}\right] u_l(r';R') + \sum_j \sum_{k=|j-l|}^{j+l} \sqrt{(2l+1)(2j+1)} \times \begin{pmatrix} j & k & l \\ 0 & 0 & 0 \end{pmatrix}^2 \frac{r'^k_<}{r'^{k+1}_>} u_j(r';R') = E(R') u_l(r';R'), \quad (3)$$

where $\begin{pmatrix} j & k & l \\ 0 & 0 & 0 \end{pmatrix}$ is the Wigner-3$j$ symbols [28,29]. To solve the eigenvalue problem, we apply the generalized pseudospectral (GPS) method [30], which provides a highly accurate differentiation matrix. The nonlinear mapping $r' = \frac{1+x+c_1}{1-x+c_2}$, $x \in [-1,1]$ is used, where $c_1$ and $c_2$ are determined by the $r'$ range with $r'_{\min} = 10^{-15}$ and $r'_{\max} = 200$ adopted here, together with $u_l(r'(x)) = \sqrt{\frac{dr'(x)}{dx}} g_l(r'(x))$ as explained in Ref. [30]. The Legendre-Gauss-Lobatto grids are used in calculation [31], i.e., $\{x_k\}_{k=2}^{N-1}$ the zeros of $\frac{d}{dx}P_{N-1}(x_k)$ with $x_{1,N} = \mp 1$, where $P_{N-1}(x)$ is the Legendre polynomial with $N$ being the number of grids that we use $N = 201$ here. After discretization, the coupled Eq. (3) can be written as $(N-2)\times(l_{\max}+1)$ matrix equation with the column vector $\mathbf{u}^T = [u_0(x_2), u_0(x_3), \ldots, u_0(x_{N-2}), \ldots, u_{l_{\max}}(x_2), u_{l_{\max}}(x_3), \ldots, u_{l_{\max}}(x_{N-2})]$, where $l_{\max}$ denotes the maximum angular quantum number and with the boundary conditions $u_l(x_{1,N}) = 0$. The electronic wave function converges as $l_{\max}$ increases. Here we use $l_{\max} = 7$, which is calibrated by comparing the calculated electronic potential energies with the results of Shimamura [9]. Table I shows an excerpt of the results at $1\sigma$ and $2\sigma$ states. The difference between Shimamura's and ours is less than $10^{-4}$ for $1\sigma$, and the accuracy of the $2\sigma$ state is better than that of the $1\sigma$ state. The validity of $l_{\max}$ is also examined by the accuracy of the hadron eigenenergy $\varepsilon$. Substituting $\chi(\mathbf{R}') = \frac{f(R')}{R'} Y_{l_x m_x}(\Omega_{\mathbf{R}'})$ into Eq. (2b) yields

$$-\frac{1}{2M_r}\frac{\partial^2}{\partial R'^2} f(R') + \left[\frac{l_x(l_x+1)}{2M'_r R'^2} + E_g(R') - \frac{2}{R'}\right] f(R') = \varepsilon f(R'), \quad (4)$$

where $l_x$ is equal to $n_x - 1$ with $n_x = (M_r)^{1/2}$ for the circular states [1,3,8,32], and $E_g(R')$ is the electronic ground-state eigenenergy of Eq. (3). For antiprotons, the eigenenergies we obtained are $-2.80031$ ($l_{\max} = 7$) and $-2.80033$ ($l_{\max} = 8$), whereas for kaons, the eigenenergies are $-2.80013$ ($l_{\max} = 7$) and $-2.80015$ ($l_{\max} = 8$), where the GPS method is applied with $R'_{\min} = 10^{-15}$ and $R'_{\max} = 10$. Both hadrons show the accuracy of eigenenergies at the fourth digit in mantissa, which is sufficient for the strong-field calculations. The two kinds of hadronic circular-state wave functions considered here are shown on the right axis of Fig. 2, whereas the left axis denotes the hadronic potential. The hadronic wave functions are used to estimate the average distance $\langle R'\rangle$, which determines the electronic ionization energy $I_p = E_g(\langle R'\rangle)$ and the rotation period of the hadron $T_{\rm rot} = 2\pi\langle R'\rangle/\langle v'\rangle$. The hadronic velocity $\langle v'\rangle$ is determined by the hadronic kinetic energy $\frac{\langle \mathbf{p}^2\rangle}{2M_r}$, where $M_r$ is compiled in Refs. [33,34]. The list of parameters used for the two targets before ($X^-He^+$) and after ($X^-He^{2+}$) electronic ionization is shown in Table II. After electronic ionization, the hadron experiences a stronger attractive force from the helium nucleus ($+2e$) than that before ionization ($+e$). Thus, the average distance $\langle R'\rangle$ after ionization becomes shorter and the rotation speed of the hadron is faster than that before ionization. In our paper, the electronic motion driven by the laser field is calculated with $R'$ fixed at $\langle R'\rangle$.

TABLE II. Parameters of negative hadronic helium atoms and ions. $(n_x,l_x)$ are principal and azimuthal quantum numbers of the most probable circular states in the hydrogenic model. $M_r$ is the reduced mass of the hadron and helium nucleus. $\langle R'\rangle$ is the averaged distance of the hadron to nucleus of the circular state. $I_p$ is the electron ionization potential. $T_{\rm rot}$ is the hadron rotation period in femtosecond and $\omega_{\rm rot}$ is the rotation frequency in eV.

| Hadronic atom | $(n_x,l_x)$ | $M_r$ (a.u.) | $\langle R'\rangle$ (a.u.) | $I_p$ (a.u.) | $T_{\rm rot}$ (fs) | $\omega_{\rm rot}$ (eV) |
|---|---|---|---|---|---|---|
| $\bar{p}He^+$ | (38,37) | 1466.8986 | 0.5749 | 0.8037 | 1.9097 | $2.1656(\sim 1.4\omega_{\rm IR})$ |
| $\bar{p}He^{2+}$ | – | – | 0.4987 | – | 1.4407 | $2.8707(\sim 1.9\omega_{\rm IR})$ |
| $K^-He^+$ | (29,28) | 853.1106 | 0.5791 | 0.8071 | 1.4694 | $2.8144(\sim 1.8\omega_{\rm IR})$ |
| $K^-He^{2+}$ | – | – | 0.5014 | – | 1.1055 | $3.7411(\sim 2.4\omega_{\rm IR})$ |

### B. Coordinates transformation

The wave function in the rotating frame $S'$ is now transformed back to the laboratory frame $S$. The transformation can be described by the rotation operator $\widehat{R}(\hat{\vartheta})$, where $\hat{\vartheta} = (\alpha,\beta,\gamma)$ is the Eulerian angle [29]

$$\varphi_{jm}(\widehat{\mathbf{r}}) = \sum_{j'm'} \langle j'm'|\hat{R}(\hat{\vartheta})|jm\rangle \varphi_{j'm'}(\widehat{\mathbf{r}}) = \sum_{m'} D^{j}_{m'm}(\hat{\vartheta})\varphi_{jm'}(\widehat{\mathbf{r}}), \quad (5)$$

where $D^{j}_{m'm}(\hat{\vartheta}) = \langle jm'|\widehat{R}(\hat{\vartheta})|jm\rangle$ is the rotation matrix and the summation index $j'$ is excluded later because the total angular momentum is unaltered during the rotation transformation. By designating the rotation of $\widehat{R}(\hat{\vartheta})$ that transforms $P_1(\theta_1,\phi_1)$ and $P_2(\theta_2,\phi_2)$ to $P_1'(\theta_1',\phi_1')$ and $P_2'(\theta_2',\phi_2')$ in a unit sphere, respectively, the orthogonality of $D^{j}_{m'm}(\hat{\vartheta})$ can provide the identity [29]

$$\sum_m Y^*_{jm}(\theta_1,\phi_1)Y_{jm}(\theta_2,\phi_2) = \sum_m Y^*_{jm}(\theta_1',\phi_1')Y_{jm}(\theta_2',\phi_2'). \quad (6)$$

In the $S'$ frame we simply set the hadron at $(\theta_1' = 0,\phi_1' = 0)$, and the electron at $(\theta',\phi')$. By using $Y^*_{jm}(0,0) = \sqrt{\frac{2j+1}{4\pi}}\delta_{m0}$ we obtain

$$Y_{j0}(\theta',\phi') = \sqrt{\frac{4\pi}{2j+1}}\sum_m Y^*_{jm}(\theta_1,\phi_1)Y_{jm}(\theta_2,\phi_2). \quad (7)$$

Comparing Eq. (7) with Eq. (5) thus gives $D^{j}_{m0}(\vartheta) = \sqrt{\frac{4\pi}{2j+1}}Y^*_{jm}(\theta_1,\phi_1)$. We assume the classical orbiting motion [1] of the hadron nucleus at large angular momentum $l_x$ with the rotation angle $\theta_1 = \theta_{\rm rot}(t) = \omega_{\rm rot}t + \theta_0$ and $\phi_1 = 0$ according to Fig. 1(a). The ground-state electronic wave function in the laboratory frame $S$ can be written as

$$\psi(\mathbf{r}';\mathbf{R}') = \sum_j \frac{u_j(r';R')}{r'}Y_{j0}(\theta',\phi') = \sum_{jm_j} \frac{u_j(r;R)}{r}Y_{jm_j}(\theta,\phi)\sqrt{\frac{4\pi}{2j+1}}Y^*_{jm_j}(\theta_{\rm rot},0) = \sum_{jm_j}\psi_{jm}(\mathbf{r};\mathbf{R})R_{jm_j}(\theta_{\rm rot}), \quad (8)$$

where $\psi_{jm}(\mathbf{r};\mathbf{R}) = \frac{u_j(r;R')}{r}Y_{jm_j}(\theta,\phi)$ and $R_{jm_j}(\theta_{\rm rot}) = \sqrt{\frac{4\pi}{2j+1}}Y^*_{jm_j}(\theta_{\rm rot},0)$ called the rotation factor here, which is useful to elucidate the rotation effects in Sec. III.

### C. Electronic excitation by intense field

With the presence of a strong IR field, the electron in the hadronic helium can be excited into a continuum, rescattered with a parent ion, and then emits a high-order harmonics [35]. In contrast, the excitation of the hadron can be neglected because of a much heavier hadronic mass than the electron mass. Figure 1(c) shows a schematic diagram of an interaction of the hadronic helium with an IR electric field. In this paper we consider the linearly polarized light pulse. We assign the polarization direction as the $z$ axis ($\theta_E = 0$) for convenience. If we choose $\theta_E \neq 0$, there will be a factor difference of $\cos\gamma$ [described below Eq. (11)] in transition amplitude Eq. (11) between the two conventions and the factor is time independent. Hence this assumption will not affect the physical

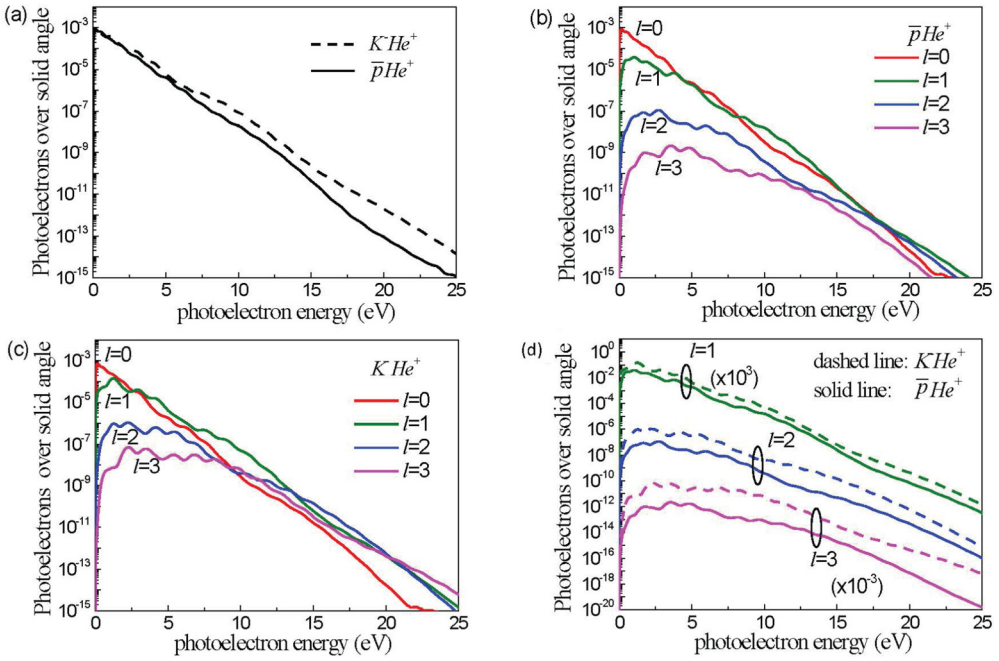


FIG. 3. (Color online) (a) ATI spectra of the $\overline{p}He^+$ atom (black-solid line) and the $K^-He^+$ atom (black-dashed line). Decomposed ATI spectra of (b) the $\overline{p}He^+$ atom and (c) the $K^-He^+$ atom by the angular quantum number from $l = 0$ to $l = 3$. (d) Comparison between decomposed ATI spectra of the $\overline{p}He^+$ atom (solid line) and the $K^-He^+$ atom (dashed line). $\lambda_{\rm IR} = 800$ nm, $I_{\rm IR} = 5\times10^{14}$ W/cm$^2$, and $\tau_{\rm IR} = 5$ fs.

interpretation for the circular-state effect on the ATI and HHG spectra.

The electronic excitation process can be described by the interaction potential $V_{\rm IR}(t) = \mathbf{A}_{\rm IR}(t)\cdot\mathbf{p}/c + \mathbf{A}^2_{\rm IR}(t)/2c^2$ with

$$\mathbf{A}_{\rm IR}(t) = \widehat{\varepsilon}\frac{cE_{\rm IR}}{\omega_{\rm IR}}\exp\left[-2\ln 2\left(\frac{t}{\tau_{\rm IR}}\right)^2\right]\cos(\omega_{\rm IR}t), \quad (9)$$

where $\omega_{\rm IR} = 1.55$ eV (800 nm) and $\tau_{\rm IR} = 5$ fs were used as an example. The unit vector $\widehat{\varepsilon}$ is defined in Fig. 1(c).

The ionized ground-state electron is described by the Volkov wave as

$$\left|\phi^V_{\mathbf{k}}(t)\right\rangle = \phi_{\mathbf{k}}(\mathbf{r})\exp\left[-i\int_{-\infty}^{t}E_{\mathbf{k}}(t')dt'\right], \quad (10)$$

where $\phi_{\mathbf{k}}(\mathbf{r}) = (2\pi)^{-3/2}\exp(i\mathbf{k}\cdot\mathbf{r})$ and $E_{\mathbf{k}}(t') = \frac{1}{2}[\mathbf{k} + \mathbf{A}_{\rm IR}(t)/c]^2$.

According to the $S$-matrix theory [36–39], the first-order transition amplitude can be written as

$$\begin{aligned} T_{\mathbf{k}}(t) &= -i\int_{t_i}^{t}dt_1\left\langle\phi^V_{\mathbf{k}}(t_1)\right|V_{\rm IR}(t_1)|\psi_g(t_1)\rangle \\ &= -i\int_{t_i}^{t}dt_1\left\langle\phi^V_{\mathbf{k}}(t_1)|V_{\rm IR}(t_1)|\sum_{lm_l}\psi_{lm_l}(t_1)R_{lm_l}(\theta_{\rm rot})\right\rangle, \end{aligned} \quad (11)$$

and the photoelectron (ATI) spectrum $\partial P(E)/\partial E$ is calculated by $\int_{\rm all\ \Omega_k}|T_{\mathbf{k}}(t_f)|^2 k d\Omega_k$. Here we can see the transition amplitude with $\theta_E \neq 0$ differs from that with $\theta_E = 0$ by the factor $\cos\gamma = \cos\theta\cos\theta_E + \sin\theta\sin\theta_E\cos(\phi - \phi_E)$, which is a time-independent term and shall not affect the circular effect caused by the rotation factor.

Regarding the HHG, by constructing the time-dependent electronic wave function

$$|\Psi(t)\rangle = |\psi_g(t)\rangle + \int d^3\mathbf{k}T_{\mathbf{k}}(t)\left|\phi^V_{\mathbf{k}}(t)\right\rangle, \quad (12)$$

the dipole moment for harmonic emission can then be calculated using

$$\begin{aligned} d(t) &\equiv \langle\Psi(t)|z|\Psi(t)\rangle \\ &= -i\int_{t_i}^{t}dt_1\int d^3\mathbf{k}\langle\psi_g(t)|z|\phi_{\mathbf{k}}\rangle\langle\phi_{\mathbf{k}}|V_{\rm IR}(t_1)|\psi_g(t_1)\rangle \\ &\quad\times\exp\left[-i\int_{t_1}^{t}E_{\mathbf{k}}(t')dt'\right] + \text{c.c.}, \end{aligned} \quad (13)$$

where c.c. means the complex conjugate, and the multiple integral is accurately calculated without using the stationary phase approximation [40]. Consequently, the HHG spectrum can be obtained through $|\text{HHG}(\omega)|^2 = |\int_{-\infty}^{\infty}d(t)\exp(-i\omega t)dt|^2$.

## III. RESULTS AND DISCUSSIONS

### A. ATI spectra of the hadronic helium atom

Figure 3(a) shows the ATI spectra of $\overline{p}\text{He}^+$ (solid line) and $K^-\text{He}^+$ (dashed line) under the laser pulse of peak intensity $3\times10^{13}$ W/cm$^2$, where the Coulomb rescattering effect can be neglected. As expected, both spectra monotonically decay with the energy, but $K^-\text{He}^+$ shows a spectrum higher than $\overline{p}\text{He}^+$. It seems inconsistent with the fact that the ionization potential of $K^-\text{He}^+$ is higher than that of $\overline{p}\text{He}^+$. The

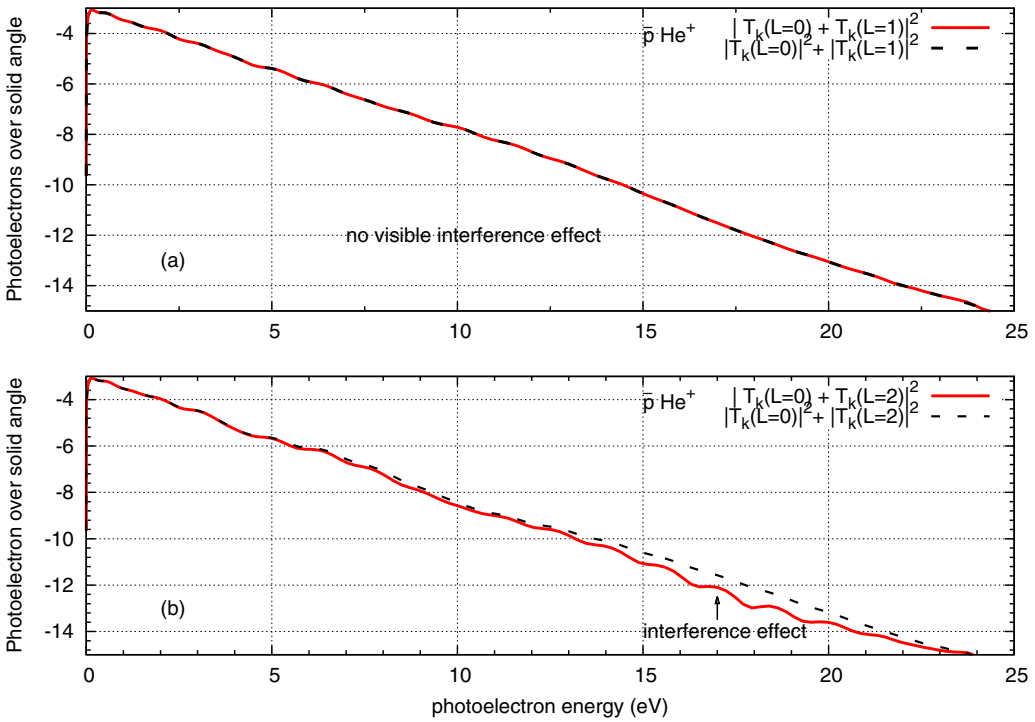


FIG. 4. (Color online) (a) Differential photoelectron spectra calculated from $|T_k(l=0) + T_k(l=1)|^2$ and $|T_k(l=0)|^2 + |T_k(l=1)|^2$ show invisible interference. (b) Corresponding plot for $l=0$ and $l=2$, interferences appear near the energy region 16 eV. The label of vertical axis is in power of 10.

results come from the effect of hadronic rotation. To reveal this effect, it is helpful to decompose the ATI spectrum by angular quantum numbers $l$. Figures 3(b) and 3(c) show the decomposed spectrum for $\overline{p}\mathrm{He}^+$ and $K^-\mathrm{He}^+$, respectively. At very low photoelectron energies, the $l=0$ spectrum is most dominant among all decomposed spectra. However, at higher photoelectron energy, this dependence changes because the $l=1$ spectrum becomes higher than the $l=0$ one. This phenomenon is particularly evident for $K^-\mathrm{He}^+$, where the crossover point is at ~3 eV. Moreover, in $K^-\mathrm{He}^+$ the $l=2$ spectrum can even overcome the $l=1$ spectrum beyond ~14 eV. The enhanced ATI spectrum is stronger in $K^-\mathrm{He}^+$ than $\overline{p}\mathrm{He}^+$ because of their different hadronic rotation speeds. Note that the convergence of enhanced ATI spectrum as $l$ increases was examined, while the spectra in Fig. 3(a) are summed up to $l_{\max}=7$ to ensure the accuracy.

The relation between the enhancement and the rotation effect can be elucidated analytically. In hadronic helium, the molecularlike structure causes the electronic ground state to have a number of orbital components, and each of these orbital components is multiplied by the rotation factor $R_{lm_l}(\theta_{\mathrm{rot}})$ because of the effect of hadronic rotation as shown in Eq. (8). The rotation factor is proportional to $Y^*_{lm_l}(\theta_{\mathrm{rot}},0)$, which reduces the effective ionization energy because of the phase term $(\omega_{kg}-l\omega_{\mathrm{rot}})t$ in the transition amplitude [Eq. (11)], where $\omega_{kg}=\omega_k-\omega_p$, $\omega_k$ is the energy of an ionized electron, and $I_p\equiv-\omega_g$ is the ionization potential. For the $l=1$ component, the effective ionization energy is reduced by $\omega_{\mathrm{rot}}$, because, for example, $Y^*_{10}(\theta_{\mathrm{rot}},0)\propto\cos\theta_{\mathrm{rot}}\propto(e^{i\omega_{\mathrm{rot}}t}+e^{-i\omega_{\mathrm{rot}}t})$, which leads to a phase term $(\omega_{kg}-\omega_{\mathrm{rot}})t=(\omega_k+I_p-\omega_{\mathrm{rot}})t$ in the transition amplitude, where $\theta_0$ is temporarily neglected for simplicity, and so is $Y^*_{1\pm1}(\theta_{\mathrm{rot}},0)$. Similarly, for the $l=2$ component, the effective ionization energy is reduced by $2\omega_{\mathrm{rot}}$, and so on. Because the kaon has a smaller mass than the antiproton, the rotation speed of $K^-\mathrm{He}^+$ is faster than that of $\overline{p}\mathrm{He}^+$. Thus, the enhancement caused by the rotation factor is more substantial in $K^-\mathrm{He}^+$ than in $\overline{p}\mathrm{He}^+$. This is particularly evident in Fig. 3(d), where the difference of ATI spectra between $K^-\mathrm{He}^+$ and $\overline{p}\mathrm{He}^+$ is multiplied as $l$ increases. The rotation effect then overcomes the difference of ionization energy between the two targets, and eventually produces a higher ATI spectrum in $K^-\mathrm{He}^+$ than in $\overline{p}\mathrm{He}^+$.

In the transition amplitude Eq. (11), various angular components $\psi_{l,m_l=0}$ contribute to a photoelectron at momentum $\mathbf{k}$. The transition amplitudes from different $l$ angular orbitals cause an interference effect. As an example, Fig. 3(b) shows the differential photoelectron spectra of $l=0$ cross $l=1$ near energy 5 eV and other energies; while $l=0,1,2$ cross near the 16 eV region. The interferences in these energy regions are possible. With the expansion of plane wave, Eq. (11) becomes

$$e^{-i\vec{k}\cdot\vec{r}}=4\pi\sum_{l,m}(-i)^l Y_{lm}(\hat{k})Y^*_{lm}(\hat{r})j_l(kr),$$

$$T_{\mathbf{k}}(t=\infty)=\frac{1}{\pi}\sum_l(-i)^{l+1}\sqrt{\frac{2l+1}{2}}P_l(\cos\theta_k)\times\int_{-\infty}^{+\infty}dt[k_zA(t)+A(t)^2/2]P_l(\cos[\omega_{\mathrm{rot}}t])\times\exp\left[i\int_{-\infty}^{t}E_{\mathbf{k}}(t')dt'+iI_pt\right]\times\int_0^\infty dr\,j_l(kr)\psi_{l0}(r). \quad (14)$$

We can see there is a factor $(-i)^{l+1}$ for $l$-component transition amplitude $T_k(l)$. Thus, $l=0$ and $l=1$ will have a minor interference effect because of the phase difference of $i$, while $l=0$ and $l=2$ may show interference. Figure 4(a) shows $|T_k(l=0)+T_k(l=1)|^2$ and $|T_k(l=0)|^2+|T_k(l=1)|^2$, there is negligible interference effect. In Fig. 4(b) we show corresponding plots for $l=0$ and $l=2$, interferences appear in the electron energy region near 16 eV.

### B. HHG spectra of the hadronic helium atom

Figure 5 shows the HHG spectrum of the $\overline{p}\mathrm{He}^+$ atom under the laser pulse at a peak intensity of $5\times10^{14}$ W/cm$^2$. At first glance, the HHG spectrum of $\overline{p}\mathrm{He}^+$ (black solid line)

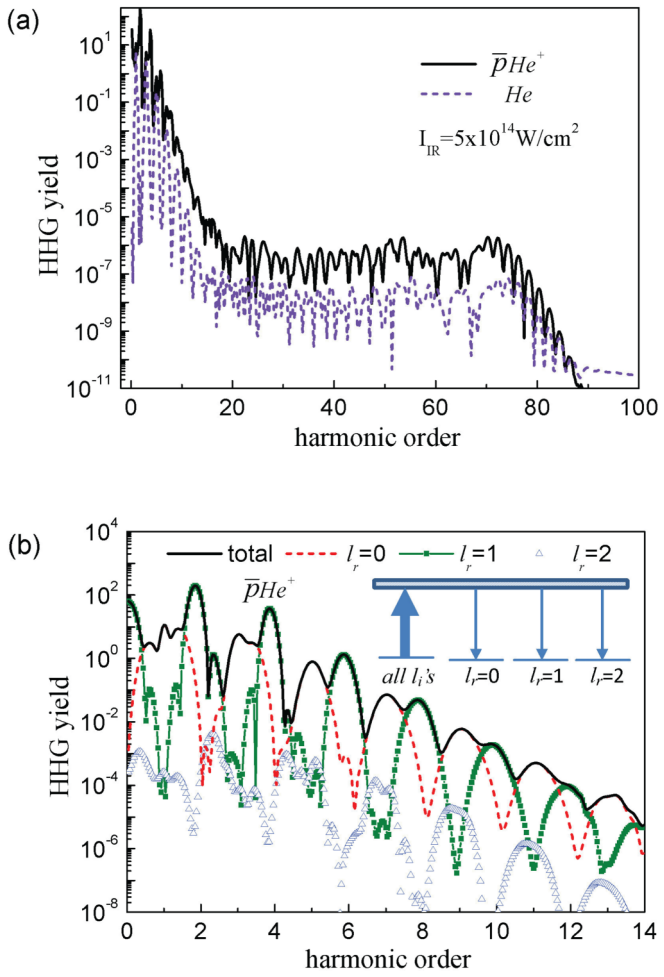


FIG. 5. (Color online) (a) HHG spectra of the $X^-\mathrm{He}^+$ atom (black solid line) and the He atom (purple dashed line). (b) Harmonic spectra of the $\overline{p}\mathrm{He}^+$ atom at first few orders (black solid line) and decomposed harmonic spectrum by the recombined orbitals $l_r=0$ (red-dashed line), $l_r=1$ (green-scatter line), and $l_r=2$ (blue-triangular scatter) with all ionized orbitals $l_i$. $\lambda_{\mathrm{IR}}=800$ nm, $I_{\mathrm{IR}}=5\times10^{14}$ W/cm$^2$, and $\tau_{\mathrm{IR}}=5$ fs.

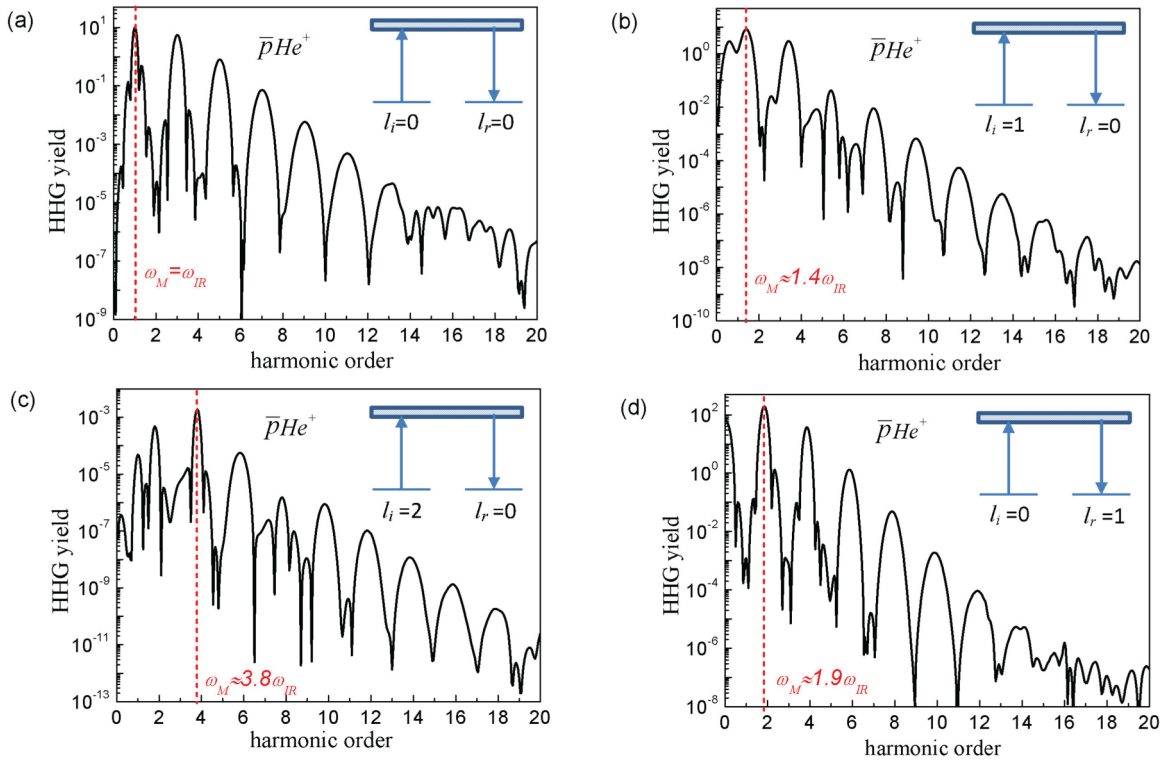


FIG. 6. (Color online) Decomposed harmonic spectra of $\overline{p}\mathrm{He}^+$ by the ionized orbital $l_i$ and the recombined orbital $l_r$ at a number of conditions to demonstrate the effect of molecularlike structure and rotation behavior, where $\omega_M$ denotes the main harmonic. (a) At $l_i = 0$ and $l_r = 0$, $\omega_M = \omega_{\mathrm{IR}}$. (b) At $l_i = 1$ and $l_r = 0$, $\omega_M = \omega_{\mathrm{rot}}(\overline{p}\mathrm{He}^+)$. (c) At $l_i = 2$ and $l_r = 0$, $\omega_M = \omega_{\mathrm{IR}} + 2\omega_{\mathrm{rot}}(\overline{p}\mathrm{He}^+)$. (d) At $l_i = 0$ and $l_r = 1$, $\omega_M = \omega_{\mathrm{rot}}(\overline{p}\mathrm{He}^{2+})$.

resembles that of the atomic helium case (purple dashed line), which can be classified into perturbative, plateau, and cut-off regions, except a larger HHG intensity in $\overline{p}\mathrm{He}^+$, because its ionization potential, is lower than that of the He atom. However, at a closer look, the HHG spectrum of $\overline{p}\mathrm{He}^+$ has a quite different fine structure from that of He atoms. As shown in Fig. 5(b), the harmonic orders of $\overline{p}\mathrm{He}^+$ are not exactly in odd integers as atomic case and also not in exact integers as that of heteronuclear diatomic molecules [41–43]. The special harmonics are due to different transitions between the continuum and the ground states as indicated, and can be interpreted below by the combined effect of the moleculelike structure with the hadronic rotation, where $l_i$ and $l_r$ denote the ionized and recombined angular orbitals, respectively.

First, we consider the effect of molecularlike structure. In such structure, since the electronic ground state involves different orbital $l$ components, the ionized orbital can be different from the recombined orbital. If the parity of an ionized orbital keeps the same as the parity of a recombined orbital [i.e., even (odd) $l_i$ and even (odd) $l_r$], emitted photons occur at odd harmonic orders, which maintains the case of atoms and homonuclear diatomic molecules with inversion symmetry. In contrast, if the parity of an ionized orbital becomes opposed to that of a recombined orbital [i.e., even (odd) $l_i$ and odd (even) $l_r$], emitted photons start occurring at even harmonic orders. This is similar to the case of heteronuclear diatomic molecules, where even harmonic orders appear because of the lack of inversion symmetry [41–43]. Next, as for the rotation effect, it can cause the shift of HHG spectra because of the rotation factor $\propto Y^*_{lm_l}(\omega_{\mathrm{rot}}t, 0)$, which contains $l$th order harmonics of frequency $\omega_{\mathrm{rot}}$. Since the harmonics can be of $\pm l\omega_{\mathrm{rot}}$, the shift can cause the HHG spectrum to a higher or lower frequency at the variant amount of $l\omega_{\mathrm{rot}}$, which is considerable because $\omega_{\mathrm{rot}}$ is comparable to $\omega_{\mathrm{IR}}$. The rotation frequency can be further classified into two types, i.e., $\omega_{\mathrm{rot}}(X^-\mathrm{He}^+)$ and $\omega_{\mathrm{rot}}(X^-\mathrm{He}^{2+})$. Before $X^-\mathrm{He}^+$ is ionized, the rotation frequency is $\omega_{\mathrm{rot}}(X^-\mathrm{He}^+)$ and the frequency shift in the HHG spectra can be expressed as $\pm l_i\omega_{\mathrm{rot}}(X^-\mathrm{He}^+)$ by Eq. (13), where the rotation contribution is due to the ionized electron state $|\psi_g(t_1)\rangle$. In contrast, after $X^-\mathrm{He}^+$ is ionized, the rotation frequency is $\omega_{\mathrm{rot}}(X^-\mathrm{He}^{2+})$ and the frequency shift in the HHG spectra can be expressed as $\pm l_r\omega_{\mathrm{rot}}(X^-\mathrm{He}^{2+})$ by Eq. (13), where the rotation contribution is due to the recombined electron state $\langle\psi_g(t)|$. Because of a stronger Coulomb force, $\omega_{\mathrm{rot}}(X^-\mathrm{He}^{2+})$ is higher than $\omega_{\mathrm{rot}}(X^-\mathrm{He}^+)$, whose magnitudes are listed in Table II.

To examine the above statements, Fig. 6 shows the HHG spectra of $\overline{p}\mathrm{He}^+$ at different orbital conditions. If an electron is ionized from the $l_i = 0$ orbital and finally recombines to the $l_r = 0$ orbital [as shown in Fig. 6(a)], the parity between the ionized and recombined orbitals remains the same (both $l_i$ and $l_r$ are even), and the rotation factor $\propto Y^*_{lm_l}(\omega_{\mathrm{rot}}t, 0)$ at $l = 0$ gives no frequency shift. Thus, the main harmonic is $\omega_M = \omega_{\mathrm{IR}}$ with subsequent harmonic orders separated by $2\omega_{\mathrm{IR}}$, which maintains the atomic or homonuclear diatomic case. Next, if the electron becomes ionized from the $l_i = 1$ orbital and finally recombines to the $l_r = 0$ orbital [as shown in Fig. 6(b)], the parity between the two orbitals now turn differently; thus,

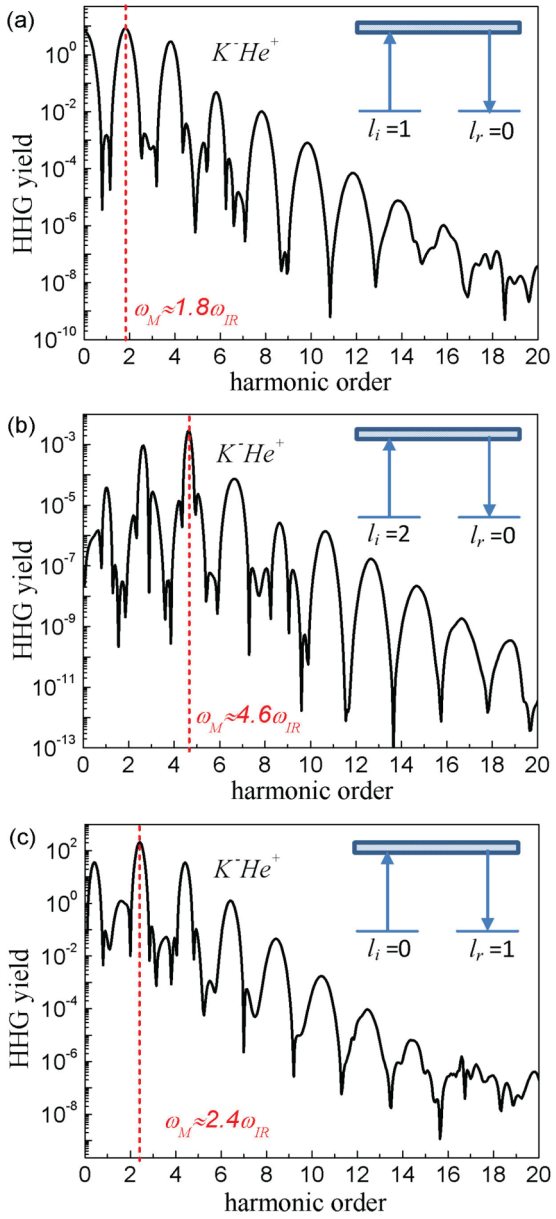


FIG. 7. (Color online) Decomposed harmonic spectra of $K^-He^+$ by the ionized orbital $l_i$ and the recombined orbital $l_r$ at a number of conditions to demonstrate the effect of molecularlike structure and rotation behavior, where $\omega_M$ denotes the main harmonic. (a) At $l_i = 1$ and $l_r = 0$, $\omega_M = \omega_{\rm rot}(K^-He^+)$. (b) At $l_i = 2$ and $l_r = 0$, $\omega_M = \omega_{\rm IR} + 2\omega_{\rm rot}(K^-He^+)$. (c) At $l_i = 0$ and $l_r = 1$, $\omega_M = \omega_{\rm rot}(K^-He^{2+})$.

the emission occurs at even harmonic order. Because the rotation factor also provides a frequency shift $\omega_{\rm rot} = 2.17$ eV ($\sim 1.4\omega_{\rm IR}$), the main harmonic occurs at $1.4\omega_{\rm IR}$, as indicated by the dashed line, with subsequent orders separated by $2\omega_{\rm IR}$. The rotation factor also provides a lower frequency shift, thus there is a minor peak at the left of the main harmonic, which is at $0.6\omega_{\rm IR}$ and this equals $(2 - 1.4)\omega_{\rm IR}$ exactly.

If the ionized orbital increases to $l_i = 2$ but $l_r = 0$ remains unchanged, the parity between the ionized and recombined orbitals recovers. Because the rotation factor has a frequency component of $2\omega_{\rm rot}$, the main harmonic shown in Fig. 6(c) occurs at $3.8\omega_{\rm IR}$ and this is exactly equal to $(1 + 2 \times 1.4)\omega_{\rm IR}$. Regarding the component of $-2\omega_{\rm IR}$, a small but visible peak at $[(3 - 2 \times 1.4) = 0.2]\omega_{\rm IR}$ is an example caused by it. Otherwise, the rotation factor contains a component of zero frequency, for example, $Y^*_{20}(\omega_{\rm rot}t, 0) \propto [3\cos^2(\omega_{\rm rot}t) - 1]$. Thus, odd harmonic orders also contribute to the spectrum. Finally, the case of $l_i = 0$ and $l_r = 1$ is considered in Fig. 6(d), which is similar to that in Fig. 6(b) except for the fact that $l_i$ and $l_r$ exchange their values with each other. In this case, because $\omega_{\rm rot}(\overline{p}He^{2+})$ is involved, which is faster than $\omega_{\rm rot}(\overline{p}He^+)$, the main harmonic becomes higher than that of Fig. 6(b) and occurs at $1.9\omega_{\rm IR}$.

To provide a further example, Fig. 7 show the decomposed harmonic spectra for $K^-He^+$. In Fig. 7(a) $\omega_M = \omega_{\rm rot}(K^-He^+) \approx 1.8\omega_{\rm IR}$, where $l_i = 1$ and $l_r = 0$. In Fig. 7(b) $\omega_M = \omega_{\rm IR} + 2\omega_{\rm rot}(K^-He^+) \approx 4.6\omega_{\rm IR}$, where $l_i = 2$ and $l_r = 0$. In Fig. 7(c) $\omega_M = \omega_{\rm rot}(K^-He^{2+}) \approx 2.4\omega_{\rm IR}$, where $l_i = 0$ and $l_r = 1$. All main harmonics are exactly at their positions according to the orbital parity and the rotation effect.

## IV. CONCLUSION

In conclusion, we study the strong-field phenomena of hadronic helium atoms by using $S$-matrix theory. The combined effect of the molecularlike structure with rotation behavior of the hadronic helium is elucidated. Because of the moleculelike structure, there is a number of angular momentum components in the electronic ground state, each one carries a rotation factor caused by the rotation behavior of $X^-He^+$. The combined effect can reduce the effective ionization energy of $X^-He^+$, and then enhances the ATI spectra. The enhancement depends on the rotation speed of $X^-He^+$. As the rotation speed increases, the enhancement grows stronger and makes the ATI spectra of $K^-He^+$ become larger than that of $\overline{p}He^+$ by overcoming the difference between ionization potentials of the two targets. The combined effect also makes HHG spectra of $X^-He^+$ unusual. Among various angular orbitals, if the parity between the ionized and recombined orbitals remains the same (e.g., $l_i$ = even and $l_r$ = even), the HHG occurs at odd harmonic orders. By contrast, if the parity between the two orbitals differs (e.g., $l_i$ = odd and $l_r$ = even), the HHG can occur at even harmonic orders. In addition to the effect of molecularlike structure, the HHG spectra are also shifted by $\pm l_i\omega_{\rm rot}(X^-He^+) \pm l_r\omega_{\rm rot}(X^-He^{2+})$ because of the hadronic rotation behavior. Consequently, the combined effect can cause broad harmonic spectra of $X^-He^+$, which is suited for applications such as the generation of a high-power single attosecond pulse.

## ACKNOWLEDGMENTS

We thank Dr. Y. Teranishi for introducing the hadronic atom to us. Many insightful comments from the anonymous referee are gratefully acknowledged. The research was supported Taiwan Ministry of Science and Technology under the Contracts of MOST 103-2112-M-009-003 and NSC 97-2811-M-009-055.

[1] T. Yamazaki, E. Widmann, R. S. Hayano, M. Iwasaki, S. N. Nakamura, K. Shigaki, F. J. Hartmann, H. Daniel, T. von Egidy, P. Hofmann, Y. S. Kim, and J. Eades, Nature (London) **361**, 238 (1993).

[2] T. Yamazaki, M. Aoki, M. Iwasaki, R. S. Hayano, T. Ishikawa, H. Outa, E. Takada, H. Tamura, and A. Sakaguchi, Phys. Rev. Lett. **63**, 1590 (1989).

[3] T. Yamazaki, N. Morita, R. S. Hayano, E. Widmann, and J. Eades, Phys. Rep. **366**, 183 (2002).

[4] The detailed list of progresses and publications can be found in the website: http://asacusa.web.cern.ch/ASACUSA/asacusaweb/main/main.shtml.

[5] S. N. Nakamura, M. Iwasaki, H. Outa, R. S. Hayano, Y. Watanabe, T. Nagae, T. Yamazaki, H. Tada, T. Numao, Y. Kuno, and R. Kadono, Phys. Rev. A **45**, 6202 (1992).

[6] G. T. Condo, Phys. Lett. **9**, 65 (1964).

[7] J. E. Russel, Phys. Rev. Lett. **23**, 63 (1969).

[8] T. Yamazaki and K. Ohtsuki, Phys. Rev. A **45**, 7782 (1992).

[9] I. Shimamura, Phys. Rev. A **46**, 3776 (1992).

[10] T. Kirchner and H. Knudsen, J. Phys. B: At. Mol. Opt. Phys. **44**, 122001 (2011).

[11] M. Iwasaki, S. N. Nakamura, K. Shigaki, Y. Shimizu, H. Tamura, T. Ishikawa, R. S. Hayano, E. Takada, E. Widmann, H. Outa, M. Aoki, P. Kitching, and T. Yamazaki, Phys. Rev. Lett. **67**, 1246 (1991).

[12] N. Morita *et al.*, Phys. Rev. Lett. **72**, 1180 (1994).

[13] R. S. Hayano, M. Hori, D. Horváth, and E. Widmann, Rept. Prog. Phys. **70**, 1995 (2007).

[14] J. S. Briggs, P. T. Greenland, and E. A. Solovév, J. Phys. B: At. Mol. Opt. Phys. **32**, 197 (1999).

[15] K. Sakimoto, Phys. Rev. A **66**, 032506 (2002); **74**, 022709 (2006); **76**, 042513 (2007); **82**, 012501 (2010).

[16] M. Hori, A. Sótér, D. Barna, A. Dax, R. Hayano, S. Friedreich, B. Juhász, T. Pask, E. Widmann, D. Horváth, L. Venturelli, and N. Zurlo, Nature (London) **475**, 484 (2011).

[17] V. I. Korobov, Phys. Rev. A **77**, 042506 (2008).

[18] X. M. Tong, K. Hino, and N. Toshima, Phys. Rev. Lett. **101**, 163201 (2008).

[19] X. M. Tong and N. Toshima, Phys. Rev. A **85**, 032709 (2012).

[20] F. Krausz and M. Ivanov, Rev. Mod. Phys. **81**, 163 (2009).

[21] Z. Chang, *Fundamentals of Attosecond Optics* (CRC Press, Boca Raton, FL, 2011).

[22] C. I. Blaga, F. Catoire, P. Colosimo, G. G. Paulus, H. G. Muller, P. Agostini, and L. F. DiMauro, Nat. Phys. **5**, 335 (2008).

[23] L. Guo, S. S. Han, X. Liu, Y. Cheng, Z. Z. Xu, J. Fan, J. Chen, S. G. Chen, W. Becker, C. I. Blaga, A. D. DiChiara, E. Sistrunk, P. Agostini, and L. F. DiMauro, Phys. Rev. Lett. **110**, 013001 (2013).

[24] K. Krajewska, I. I. Fabrikant, and A. F. Starace, Phys. Rev. A **86**, 053410 (2012).

[25] D. B. Milošević, G. G. Paulus, D. Bauer, and W. Becker, J. Phys. B **39**, R203 (2006).

[26] C. D. Lin, A. T. Le, Z. Chen, T. Morishita, and R. Lucchese, J. Phys. B **43**, 122001 (2010).

[27] S. I. Chu and D. A. Telnov, Phys. Rep. **390**, 1 (2004).

[28] A. Messiah, in *Quantum Mechanics* (North Holland, Amsterdam, 1961), Vol. 2, p. 1059.

[29] V. Devanathan, *Angular Momentum Techniques in Quantum Mechanics* (Kluwer, Dordrecht, 1999).

[30] D. A. Telnov and S.-I. Chu, Phys. Rev. A **59**, 2864 (1999).

[31] J. Shen and T. Tang, *Spectral and High-Order Methods with Applications* (Science, New York, 2006).

[32] R. Landua and E. Klempt, Phys. Rev. Lett. **48**, 1722 (1982).

[33] J. Beringer *et al.* (Particle Data Group), Phys. Rev. D **86**, 010001 (2012).

[34] The mass of $He^{2+}$ ion (alpha particle) is taken from Rev. Mod. Phys. **84**, 1527 (2012).

[35] P. B. Corkum, Phys. Rev. Lett. **71**, 1994 (1993).

[36] A. Becker and F. H. M. Faisal, J. Phys. B **38**, R1 (2005).

[37] H. C. Lee, S. D. Jheng, and T. F. Jiang, J. Opt. Soc. Am. B **29**, 286 (2012).

[38] H. C. Lee and T. F. Jiang, Appl. Phys. B **109**, 621 (2012).

[39] H. C. Lee and T. F. Jiang, J. Opt. Soc. Am. B **30**, 1294 (2013).

[40] M. Lewenstein, P. Balcou, M.Y. Ivanov, A. L'Huillier, and P. B. Corkum, Phys. Rev. A **49**, 2117 (1994).

[41] J. Heslar, D. Telnov, and S.-I. Chu, Phys. Rev A **83**, 043414 (2011).

[42] J. Heslar, J. Carrera, D. Telnov, and S. I. Chu, Int. J. Quantum Chem. **107**, 3159 (2007).

[43] P. M. Kraus, A. Rupenyan, and H. J. Wörner, Phys. Rev. Lett. **109**, 233903 (2012).